Photochemistry in Dried Polymer Films Incorporating the Deionized Blue Membrane Form of Bacteriorhodopsin

Jack R. Tallent, Jeffrey A. Stuart, Q. Wang Song, Edward J. Schmidt, Charles H. Martin, and Robert R. Birge
Department of Chemistry and W. M. Keck Center for Molecular Electronics, Syracuse University, Syracuse, New York 13244-4100 USA

ABSTRACT The preparation and photochemical properties of dried deionized blue membrane ($dIbR_{600}$; $\lambda_{max} \approx 600$ nm, $\epsilon \approx 54,760\ cm^{-1}\ M^{-1}$, $f \approx 1.1$) in polyvinyl alcohol films are studied. Reversible photoconversion from $dIbR_{600}$ to the pink membrane ($dIbR_{485}$; $\lambda_{max} \approx 485$ nm) is shown to occur in these films under conditions of strong 647-nm laser irradiation. The pink membrane analog, $dIbR_{485}$, has a molar extinction coefficient of $\sim 39,000\ cm^{-1}\ M^{-1}$ ($f \approx 1.2$). The ratio of pink $\rightarrow$ blue and blue $\rightarrow$ pink quantum efficiencies is 33 ± 5. We observe an additional blue-shifted species ($dIbR_{455}$, $\lambda_{max} \approx 455$ nm) with a very low oscillator strength ($f \approx 0.6$, $\epsilon \approx 26,000\ cm^{-1}\ M^{-1}$). This species is the product of fast thermal decay of $dIbR_{485}$. Molecular modeling indicates that charge/charge and charge/dipole interactions introduced by the protonation of ASP_{85} are responsible for lowering the excited-state all-*trans* $\rightarrow$ 9-*cis* barrier to $\sim$6 kcal mol^{-1} while increasing the corresponding all-*trans* $\rightarrow$ 13-*cis* barrier to $\sim$4 kcal mol^{-1}. Photochemical formation of both 9-*cis* and 13-*cis* photoproducts are now competitive, as is observed experimentally. We suggest that $dIbR_{455}$ may be a 9-*cis*, 10-s-distorted species that partially divides the chromophore into two localized conjugated segments with a concomitant blue shift and decreased oscillator strength of the λ_{max} absorption band.

INTRODUCTION

Bacteriorhodopsin (MW $\cong$ 26,000) (bR) is the light-harvesting protein contained within the purple membrane of the salt marsh bacterium *Halobacterium salinarium* (also called *Halobacterium halobium*) (Oesterhelt and Stoeckenius, 1971, 1974; Oesterhelt and Schuhmann, 1974; Stoeckenius and Bogomolni, 1982; Birge, 1990a, 1994; Henderson et al., 1990; Mathies et al., 1991; El-Sayed, 1992; Oesterhelt et al., 1992; Ebrey, 1993; Tributsch and Bogomolni, 1994; Lanyi, 1995). The purple membrane consists of a semicrystalline protein trimer in a phospholipid matrix (3:1 protein/lipid), which constitutes a specific functional site as a proton pump in the plasma membrane of the bacterial cell. The protein has seven *trans*-membrane α-helices that make up the secondary structure. The bacterium synthesizes the purple membrane when dissolved oxygen concentrations become too low to sustain aerobic ATP production. The production of the purple membrane allows the organism to switch from oxidative phosphorylation to photosynthesis as a means of energy production.

The native protein binds $\sim$4 mol Ca(II) and Mg(II)/mol protein at pH 6.0 (Chang et al., 1986, 1987, 1988; Zhang et al., 1992). Displacement or removal of these cations results in a reversible color change from purple to blue, indicating the formation of the *blue membrane* ($\lambda_{max} \approx 600$ nm) (Kimura et al., 1984; Chang et al., 1986, 1988; Duñach et al., 1988; Jonas and Ebrey, 1991; Zhang et al., 1992). Cation displacement can be accomplished by either acidification of the purple membrane to produce the *acid blue membrane* (Fischer et al., 1981; Maeda et al., 1981; Kimura et al., 1984; Chang et al., 1987) or cation removal at standard pH to produce the *deionized blue membrane* or $dIbR_{600}$ (Chang et al., 1986, 1987, 1988; Liu and Ebrey, 1987a; Zhang et al., 1993; Birge et al., 1996). There are two different perspectives on the importance of studying the photophysical properties of $dIbR_{600}$. The blue membrane displays photochemical properties that are significantly different from the purple membrane, and thus an analysis of the photochemistry of $dIbR_{600}$ may provide insights into the relevance of the cations in mediating the photochemical and electrostatic properties of the binding site (Fischer et al., 1981; Maeda et al., 1981; Kimura et al., 1984; Chang et al., 1986, 1987, 1988; Pande et al., 1986; Chung-Ho et al., 1987; Corcoran et al., 1987; Liu and Ebrey, 1987a; Renk et al., 1987; Toth-Boconadi et al., 1989; Zhang et al., 1993; Wu and El-Sayed, 1994; El-Sayed et al., 1995; Birge et al., 1996). The observation that $dIbR_{600}$ undergoes reversible photochemistry to produce a long-lived blue-shifted photoproduct, the *pink membrane* ($\lambda_{max} \approx 490$ nm), has prompted researchers to study potential photochromic device applications (Hampp et al., 1992; Gross et al., 1995; Tallent et al., 1996; Birge et al., 1997). Our initial interest in $dIbR_{600}$ was prompted by both considerations, and our development of a low-moisture-content polyvinyl alcohol thin film was prompted by the potential of using bacteriorhodopsin as the photoactive component in holographic memories (Birge, 1990b; Curtis and Psaltis, 1992; Gu et al., 1992; Qiao and Psaltis, 1992; Heanue et al., 1994).

Both bR and $dIbR_{600}$ contain a mixture of all-*trans* and 13-*cis*, 15-*syn* species at room temperature. Light adaptation of bR converts the dark-adapted mixture ($\sim$60% 13-*cis*, $\sim$40% all-*trans*, $5 < pH < 10$) to nearly pure all-*trans* ($>$95%, $5 < pH < 10$) (Koyama et al., 1993). These authors have studied the acid blue membrane and observe that the

Received for publication 17 October 1997 and in final form 22 June 1998.
Address reprint requests to Dr. Robert R. Birge, Department of Chemistry, Syracuse University, 111 College Place, Syracuse, NY 13244-4100. Tel.: 315-443-1900; Fax: 315-443-4070; E-mail: rbirge@syr.edu.

0006-3495/98/10/1619/16 $2.00

dark-adapted species contains an enhanced amount of the all-*trans* species (~60% all-*trans*, ~40% 13-*cis*, pH < 2.5), but that light adaptation has no appreciable influence on the relative populations. The primary event in bR involves an all-*trans* → 13-*cis* photoconversion, and subsequent dark reactions are responsible for the vectorial proton translocation through the purple membrane. The quantum yield of the primary event is ~0.65 (Tittor and Oesterhelt, 1990; Ebrey, 1993). No stable photoproducts at ambient temperature are formed upon irradiation of bR, although there is a branched-photocycle pathway from the O state to form a stable 9-*cis* photoproduct (Popp et al., 1993). Less is known about the photochemistry of the blue membrane. A kinetic study by Ohtani et al. (1986) concludes that absorption of light by the blue membrane initiates a less efficient ($\Phi \approx 0.1$) primary event involving all-*trans* → 13-*cis* photoconversion followed by a truncated photocycle that includes only K- and L-like species. The single most interesting feature of both acid blue membrane and $dIbR_{600}$ is the fact that sustained irradiation yields one or more stable blue-shifted photoproducts. Although a number of studies have been carried out to characterize these blue-shifted species, the origin and details that mediate these new photochemical reactions remain a subject of debate.

The solution photochemistry of the acid-blue membrane has been studied in detail (Mowery et al., 1979; Fischer et al., 1981; Maeda et al., 1981; Chronister and El-Sayed, 1987). A majority of studies suggest that the long-lived species have a 9-*cis* conformation, and the key photochemical and thermal transformations are summarized in Fig. 1. The deionized blue membrane has also been studied, but over a much smaller pH range because of the difficulty of manipulating pH without introducing cations (Pande et al., 1986; Chang et al., 1987; Chung-Ho et al., 1987; Liu and Ebrey, 1987a; Toth-Boconadi et al., 1989). The vast majority of the previous studies have been carried out in solution or hydrated gels; studies of dried films are largely absent. The probable reason for this is the difficulty in fabricating such films; upon drying, the deionized blue membrane exhibits a strong tendency toward reversion to the purple membrane, due presumably to cationic contamination. It should be noted, however, that brief mention of dried pink membrane films appears in the literature, consistent with the fact that the pink membrane is insensitive to the presence of cations (Chang et al., 1987). Also, Renthal and Regalado (1991) have studied the absorption spectra of acid (pH < 1) blue membrane films, noting that the absorption maximum shifts from 600 to 578 nm upon vacuum dehydration at 0.1 torr.

The goal of this study was to fabricate and characterize the photochromic properties of dried deionized polymer/blue membrane films. The resulting films display unusual photophysical properties, which are described below. Theoretical analysis of the results provides new insights into the observed photochemistry, and the role that electrostatic interactions within the protein binding site play in directing photochemical isomeric preferences.

EXPERIMENTAL

Preparation of the deionized blue membrane

Several methods for the preparation of blue membrane appear in the literature, which include treatment with strong cation exchange resins (Kimura et al., 1984), washing with EDTA (Chang et al., 1985, 1987), addition of anions (Kamo et al., 1987), electrolysis (Liu and Ebrey, 1987a) or extensive washing with distilled water. We adopted the method proposed by Chang et al. (1985, 1987). It involves the use of a buffered EDTA solution followed by moderate amounts of centrifugation, and is summarized below.

Concentrated purple membrane is pelleted (30,000 rpm for 30 min in a Beckman TI 45 rotor), resuspended in 10 mM EDTA/50 mM Tris-HCl, pH 8.0, and allowed to incubate for several hours. After this step is repeated at least once to ensure complete removal of cations by EDTA (especially calcium), the purple membrane is washed (pelleted as above) by resuspending in distilled deionized water. The sample is washed in this manner until the absorption maximum reaches 603–605 nm, although the sample will start to appear blue at 585 nm. For a large sample of purple membrane (300–500 mg), 20–25 washes in distilled deionized water are necessary.

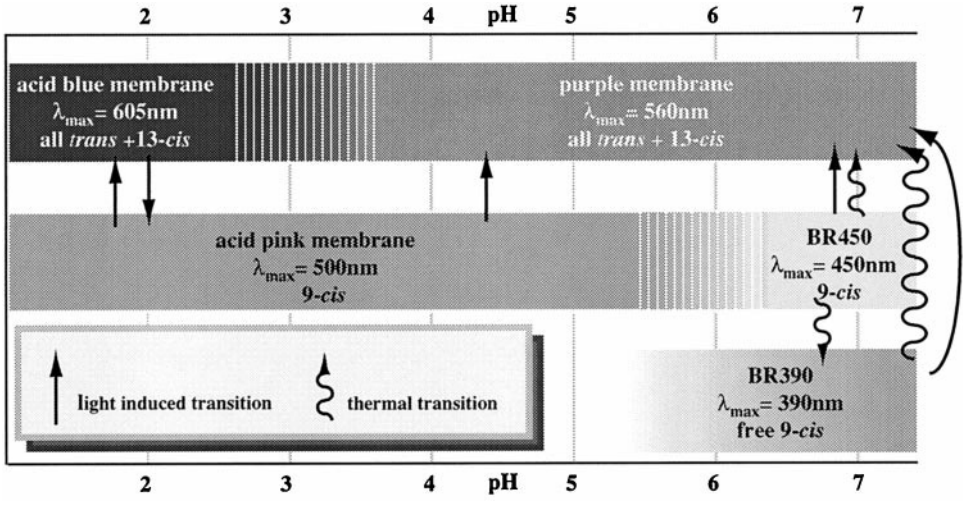

FIGURE 1 The photochemical and thermal interconversions among the family of long-lived intermediates of the acid blue membrane (after Fischer et al., 1981).

Fabrication of dried polymer/blue membrane films

Polymer-based $dIbR_{600}$ films were prepared by suspension of the protein in a deionized polymer matrix. The deionized blue membrane is very sensitive to the presence of cations, and will readily convert back to purple membrane if not rigorously isolated from the environment before drying. All materials (e.g., glassware and/or plastic implements) that come into contact with the deionized protein must be rigorously cleaned and free of cationic contaminants. This was routinely done by soaking in either an EDTA solution or a suspension of cation-exchange resin, followed by rinsing in distilled-deionized water. Although film fabrication was tried with several different polymer supports, poly(vinyl alcohol) (PVA) proved to be the most successful. Before addition of blue membrane, 100 ml of a solution of 10% PVA (wt/vol, mol wt distribution 31–50 kD, Aldrich, Milwaukee, WI, 36,313-8) was stirred for 3 h with a few grams of cation exchange resin (AG 50W-X8 resin, 100–200 mesh, hydrogen form, Bio-Rad, Hercules, CA, 142-1441). This serves to remove cation impurities, as well as drop the pH of the polymer solution (blue membrane is less likely to revert to purple at low pH). The ion exchange resin is subsequently removed from the polymer solution via centrifugation.

Deionized blue membrane was added to the deionized PVA in the form of a pellet produced by centrifugation at 30,000 rpm for 30 min using a Beckman TI-45 rotor. The supernatant was decanted and 1 ml of the thick pellet was carefully pipetted into 4 ml deionized PVA: the volumes of blue membrane pellet and PVA solution were varied, depending upon the desired optical density of the resultant dried film. The solution was mixed thoroughly, sonicated, and filtered. Before sonication (with a tip sonicator), a small amount of cation exchange resin was added to the solution to scavenge any cationic impurities introduced during subsequent processing. The solution was filtered (5 μm pore size, syringe-type filter), and mildly degassed using a small vacuum pump. Approximately 1 ml of the resulting blue membrane/polymer solution was then pipetted onto a BK-7 glass disk (one inch diameter, treated with cation exchange resin and distilled-deionized water), which was then placed in a plastic desiccator (without desiccant), acting as a dust shield. The films were dried in the desiccator at 4°C for two to three days. Reversion of $dIbR_{600}$ to bR during the drying process occurred often, and the source of the cations responsible was never identified with confidence. However, we have noted that samples prepared within plastic cuvettes are much more stable. Thus, we anticipate that the migration of internal ions within the BK-7 glass may be responsible for a significant portion of the observed reversion. More stringent cleaning of the glass plates improved stability, but was not a complete solution. Only ~10–15% of the total number of films produced remained fully blue upon drying. After drying, however, the films proved to be remarkably stable and long-lasting. The resulting films were sealed with a second BK-7 glass plate and mineral oil (as an index-matching agent), and placed in a retainer that facilitated the use of an optical mount for experimentation. Successfully dried films typically exhibited a λ_{max} of ~600 nm, indicating practically no reversion to the purple membrane.

The absorption spectrum of the acid blue membrane films is sensitive to humidity (Renthal and Regalado, 1991). Our film-drying process took place under nominal room humidity, and to a first approximation the humidity of the films can be estimated to be ~60%. We did not use vacuum dehydration, as was the case in the Renthal and Regalado study, and no change was observed in the absorption spectrum as a result of the drying process. The pH of the films could not be measured, but based on the pH of the solutions before drying, the dried film pH is estimated to be in the range $3 \leq pH \leq 4$. It is noted that the simple act of removing the cations induces a lowering of the solution pH.

Spectroscopic characterization

To observe the spectroscopic changes that occur in a $dIbR_{600}$/polymer film in response to intense laser illumination, an apparatus capable of acquiring visible wavelength absorption spectra of a small spot in the film at various times during the exposure is required. The apparatus shown in Fig. 2 was designed especially for this application, and is capable of providing spectra for exposed areas of ~1 mm^2. The spectrophotometer system utilizes a SPEX HR-320 monochromator with a 150 g/mm grating. The detector is a multi-stage Peltier thermoelectric-cooled, intensified CCD array (Princeton Instruments ICCD576S/RBTHX). The measuring light is provided by a 50 W, high-pressure mercury-xenon lamp (Spectral Energy LPS 251SR), which is focused through a small aperture, and then relay-imaged with a 4f system onto the film. The light is then focused onto the monochromator entrance slit. (The spectrophotometer therefore analyzes only light that has passed through this very small area of the film.) Coincident with the white measuring light at the film is a krypton-ion laser beam (λ = 647 nm). The laser beam intersects the film at a shallow angle to bypass the optics that recollimate the white light onto the entrance slit of the monochromator. Three mechanical shutters are used in the apparatus. One shutter blocks the light source, opening only when spectral scans of the film are occurring. A second shutter regulates exposure of the film to the laser beam, controlling the exposure duty cycle. This shutter is closed during spectral acquisition. The third shutter blocks the monochromator entrance slit, opening only during acquisition of a spectrum. Finally, the apparatus provides a means of heating the film to ascertain what role temperature plays in the behavior of the material.

Theoretical

Ground state calculations on the protein binding site were carried out by using MM2 molecular mechanics methods (Buckert and Allinger, 1982; Dudek and Ponder, 1995) or MNDO/PM3 all-valence electron semiempirical molecular orbital procedures (Dewar and Thiel, 1977; Stewart, 1989). The structure of the chromophore and surrounding binding site was minimized by using, as the starting point, coordinates based on electron cryomicroscopy data provided by Richard Henderson (Henderson et al., 1990; Grigorieff et al., 1996). We fixed the α-helical backbone atoms in all simulations unless otherwise noted. Excited state calculations were carried out by using both ZINDO/S molecular orbital theory (Zerner, 1990) or MNDO-PSDCI molecular orbital theory (Stuart et al., 1995; Martin et al., 1997). The ZINDO/S calculations included all single excitations from the 14 highest-energy occupied orbitals into the 14 lowest-energy virtual orbitals of the supersystem. The MNDO/CI basis set included all single and

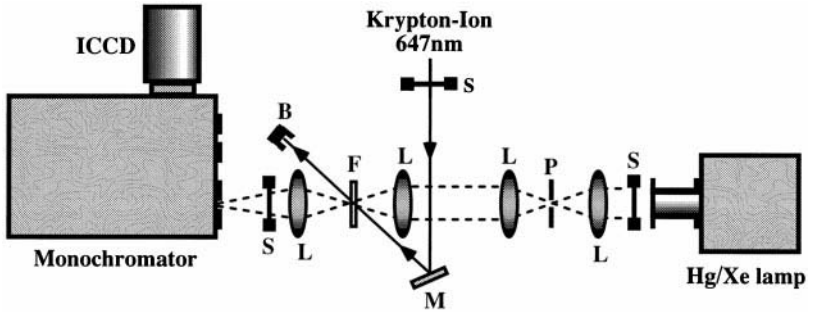

FIGURE 2 Apparatus for spectroscopic analysis of laser-induced photoconversion in dried blue membrane/PVA films. Visible light spectra can be acquired for photoproducts generated in 1-mm spots illuminated by a krypton-ion laser beam (647 nm line). The diagram is labeled as follows: ICCD, Princeton Instruments intensified CCD array; L, lens; M, mirror; p, aperture; S, mechanical shutter; B, laser beamstop; F, dried blue membrane/PVA film.

all double excitations from the π-electron system of the chromophore. Additional details of our procedures are discussed below.

RESULTS AND DISCUSSION

dIbR$_{600}$ to dIbR$_{485}$ photoconversion

Fig. 3 *a* shows the changes induced in the visible absorption spectrum of a dried dIbR$_{600}$/polymer film during the course of uninterrupted irradiation with 647 nm krypton-ion laser light. In this experiment, the actinic laser power density is relatively high, $\sim$10 W/cm^2, typical of that necessary to achieve significant photoconversion in this very insensitive material. The absence of an isosbestic point in these spectra indicates the generation of multiple products, one of which is likely denatured protein ($\lambda_{max} \approx 380$ nm).

To test the theory that denaturation is resulting from localized, laser-induced, spot heating of the film, a second experiment, the results of which are shown in Fig. 3 *b*, uses the same actinic power density, but with laser light delivered to the film in short intervals spaced by periods of darkness. The film undergoes a large number of photoactivation cycles to duplicate the same cumulative actinic light exposures as in the case of Fig. 3 *a*. In this case, periods of photoactivation last for 1 s, and are separated by 2-s intervals, during which there is no exposure to the actinic laser light. Whereas multiple products were produced in the previous experiment, interval exposure of the film to the same actinic power density for the same total exposure time results in spectral changes more indicative of a two-state system, as the near-isosbestic point suggests the production

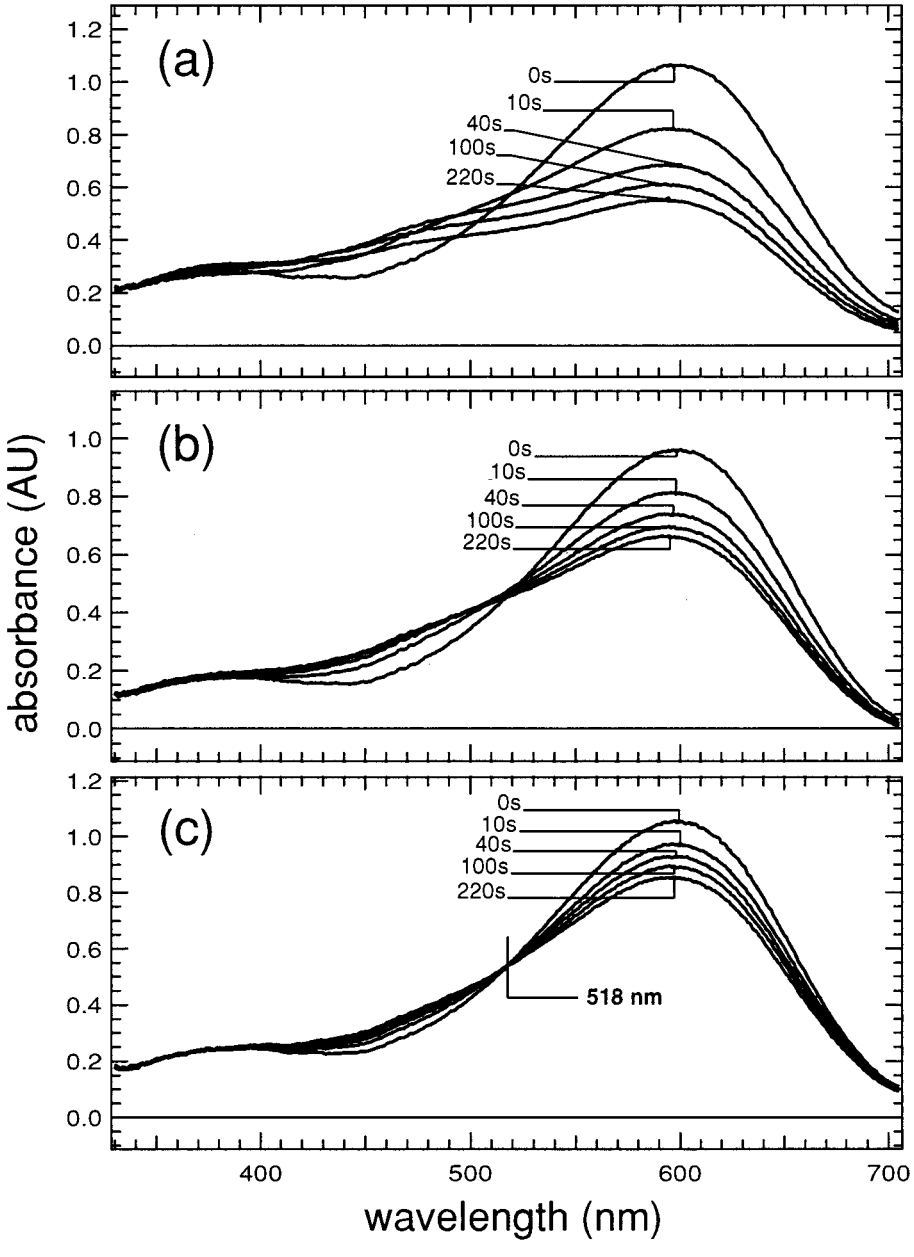

FIGURE 3 Effect of illumination interval on the photochemistry of a dried blue membrane/PVA film. (*a*) Continuous illumination. (*b*) Interval illumination 1-s on/2-s off. (*c*) interval illumination 0.5-s on/2-s off. Actinic power density is the same in each case, as is cumulative exposure.

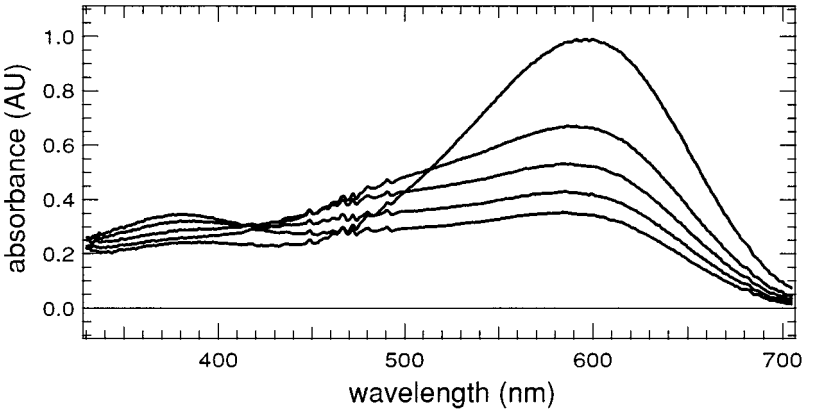

FIGURE 4 Effect of heating on photoconversion in blue membrane/polymer film. Illumination interval and actinic power density are the same as the experiment shown in Fig. 3 *c*. The film/retainer assembly is heated to ~60°C by means of a circulating bath. The resulting photochemistry is similar to that obtained from continuous illumination (see Fig. 3 *a*), supporting the hypothesis that continuous illumination produces multiple photoproducts due to localized heating.

of one major product. Further reduction of the actinic light exposure interval to 0.5 s (with 2-s darkness intervals) results in a photoconversion exhibiting an essentially perfect isosbestic point at 518 nm (Fig. 3 *c*). It should be noted once again that in each trial the actinic power density is the same, as are total exposure times.

These data support the conclusion that uninterrupted CW irradiation results in thermal products (specifically, denatured bacteriorhodopsin). The interval exposure of the film to the actinic light presumably reduces the time during which the material can be heated. This theory is further supported by the fact that if the actinic radiation is delivered to the film in such a way that otherwise avoids the generation of multiple products (as in Fig. 3 *c*), then simultaneous global heating of the film produces results similar to those obtained under CW irradiation conditions. Fig. 4 shows the changes induced in the visible absorption spectrum of a dried $dIbR_{600}$/polymer film during the course of interval actinic light exposure (using the same duty cycle as in Fig. 3 *c*) while the film temperature is maintained at ~60°C. The reduced thermal stability of the blue membrane, in comparison to the purple membrane, has been noted by other researchers (Heyn et al., 1989).

The spectra of Fig. 3 *c* indicate the generation of one photoproduct upon controlled exposure to the 647-nm actinic radiation. Shown in Fig. 5 is the calculated spectrum of this photoproduct, indicating a species with maximal absorption at ~485 nm. The observation of a long wavelength tail suggests the possibility of a small amount of blue membrane contamination. However, this tail may also be representative of spectral inhomogeneity associated with relaxation of strain within the binding site (see below). This species, hereafter referred to as $dIbR_{485}$, has a molar extinction coefficient of ~39,000 cm^{-1} M^{-1} (oscillator strength, f, ~1.2). [Determinations of molar extinction coefficients assume that ϵ_{max} for $dIbR_{600}$ in dried polymer film is the same as that reported for solution, namely 54,760 cm^{-1} M^{-1} (Liu and Ebrey, 1987b).] Because of similarities in λ_{max} and ϵ_{max} we conclude that this species corresponds to the pink membrane, which has been reported as the photoproduct of both acid and deionized blue membrane in aqueous or hydrated environments. Literature values of λ_{max} and ϵ_{max} for the pink membrane are ~490 nm and ~44,500 cm^{-1} M^{-1}, respectively (Liu and Ebrey, 1987b). The spectra of Fig. 3 *c* therefore demonstrate blue → pink photoconversion in a dried polymer film.

Although the low efficiency of this process requires high actinic power densities to accomplish significant conversion levels on the time scale of seconds, such power densities also present the possibility of unwanted photoproducts due to localized heating. Care should be taken, therefore, to

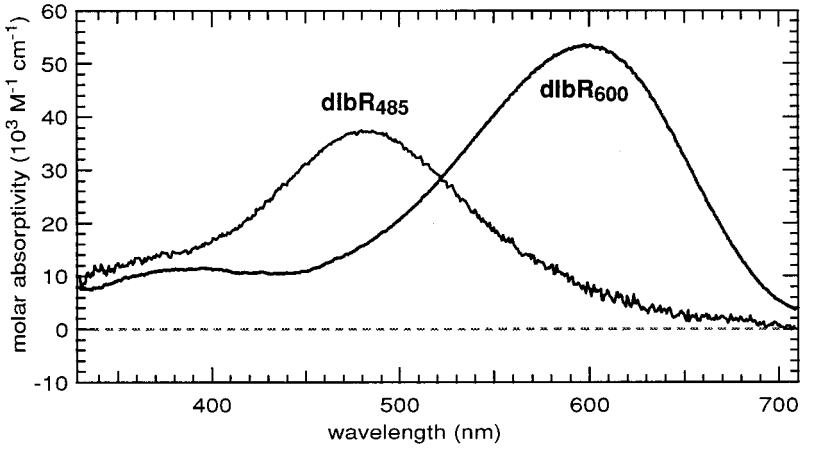

FIGURE 5 Calculated spectrum of $dIbR_{485}$, along with $dIbR_{600}$. The molar extinction coefficient of $dIbR_{485}$ is ~39,000 cm^{-1} M^{-1}, assuming a molar extinction coefficient of 54,760 cm^{-1} M^{-1} for $dIbR_{600}$.

minimize local heating effects if two-state photochromism is to be achieved in this type of material.

dIbR$_{485}$ to dIbR$_{600}$ photoconversion and quantum efficiency ratio

Fig. 6 demonstrates dIbR$_{485}$ → dIbR$_{600}$ photoconversion in a dried blue membrane/polymer film, the reverse of the process demonstrated by the spectra of Fig. 3 *c*. In this experiment, the conversion is not accomplished by actinic laser radiation, but instead occurs during the course of acquiring multiple spectra over time. The output of the broadband spectrophotometer light source exhibits high spectral power density near the reported λ_{max} of the pink membrane, and is likely responsible for driving the dIbR$_{485}$ → dIbR$_{600}$ back conversion. This reverse process exhibits an isosbestic point at the same wavelength as in the forward conversion, indicating involvement of the same two species in either case. We believe the above data constitute the first report of blue ↔ pink photochromism in a dry film.

Additionally, these data indicate the dIbR$_{485}$ → dIbR$_{600}$ conversion occurs with higher efficiency than the forward process, consistent with what has been reported for aqueous systems. We calculate the ratio of the forward ($\phi_{b\to p}$) and reverse ($\phi_{p\to b}$) quantum efficiencies with the relation:

$$(1 - x)\,\phi_{b\to p} A_b = x\phi_{p\to b} A_p, \tag{1}$$

where x is the fractional amount of photoconversion achieved at photostationary state, and A_b and A_p are the molar absorptivities of dIbR$_{600}$ and dIbR$_{485}$ at the actinic wavelength, respectively. We obtain the following result at 647 nm:

$$\frac{\phi_{p\to b}}{\phi_{b\to p}} = 33 \pm 5. \tag{2}$$

Liu and Ebrey measured a value of 55 for this ratio for photoconversion in solution (Liu and Ebrey, 1987b). Although $\phi_{p\to b}$ is much larger than $\phi_{b\to p}$ in dried films, it should be kept in mind that the absolute quantum efficiencies are much lower in the dry environment. This has been noted previously by Chang et al., with the observation that pink → blue photoconversion does not occur in dried films under actinic conditions resulting in significant conversion in aqueous environments (Chang et al., 1987).

Other photoproducts: dIbR$_{455}$

The isosbestic point in the spectra of Fig. 3 *c* indicates the presence of only one photoproduct during dIbR$_{600}$ → dIbR$_{485}$ photoconversion under the conditions described. It is important to note that this observation excludes the possibility of denaturation occurring in the film during the illumination process, a point that becomes significant in the analysis of the spectra in Fig. 7. Illustrated in Fig. 7 is the photoconversion of dIbR$_{600}$ in a dried film under conditions identical to those of Fig. 3 *c*, *with the exception that the spectrophotometer measuring light source is set to much lower intensity*. Whereas the dIbR$_{600}$ → dIbR$_{485}$ photoconversion shown in Fig. 3 *c* exhibits an essentially perfect isosbestic point at ~518 nm (consistent with that reported for aqueous systems), the photoconversion shown in Fig. 7 exhibits a near-isosbestic point that is *blue-shifted* to ~496 nm, indicating the formation of at least one photoproduct with a λ_{max} blue-shifted with respect to that of dIbR$_{485}$. One can reasonably exclude denatured protein from the possible

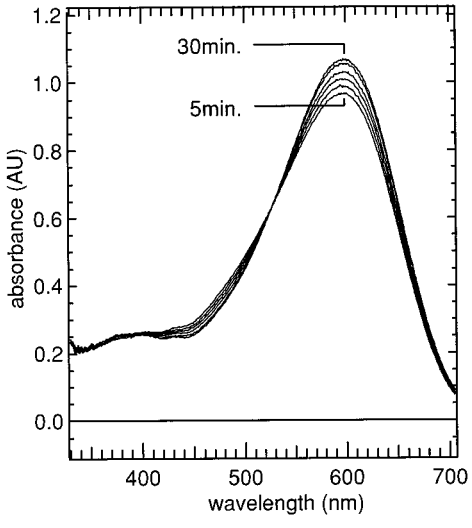

FIGURE 6 The pink-to-blue back conversion observed during the course of acquiring multiple spectra over time. The reaction is likely the result of the intense spectrophotometer measuring light, which exhibits high spectral power density near the λ_{max} of dIbR$_{485}$. The quantum efficiency for the pink → blue photoconversion is ~33 times greater than for the forward reaction.

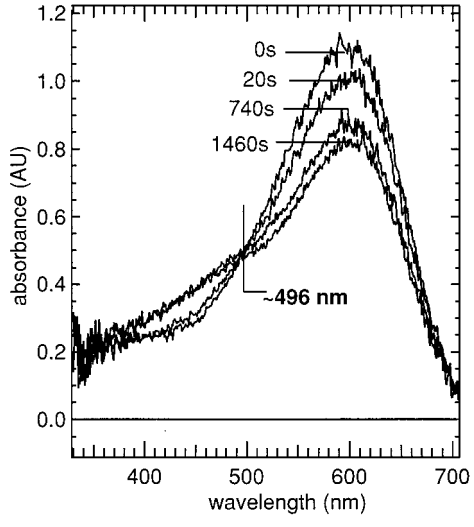

FIGURE 7 The result of interval illumination (0.5-s on/2-s off) on the photochemistry of blue membrane/PVA film under the condition of low spectrophotometer measuring light intensity. Unlike the experiment shown in Fig. 3 *c*, there is a near-isosbestic point at ~496 nm.

photoproducts, as the conditions deliver lower illumination levels to the film than were applied in the photoconversion of Fig. 3 *c*, which resulted in no denaturation.

To better characterize the blue-shifted photoproduct, the photoconversion of Fig. 7 can be treated as isosbestic and the spectra deconvoluted to produce a calculated absorption spectrum of this new blue-shifted species. Shown in Fig. 8 is the result of this deconvolution, indicating a photoproduct, hereafter designated $dIbR_{455}$, exhibiting maximal absorption in the 450–460 nm range. An unusual attribute of this calculated absorption spectrum is that it characterizes a species with an unexpectedly low molar extinction coefficient: ~26,000 cm^{-1} M^{-1} and oscillator strength ($f \approx 0.6$). Indeed, theoretical simulations based on both MNDO-PSDCI (Martin and Birge, 1998) and ZINDO-SCI (Zerner, 1990) methods suggests that this species could not be a nontorsionally distorted hexaene-protonated Schiff base. The implications of this observation are explored in more detail below.

Correlation of $dIbR_{455}$ with previously reported 450 nm absorbing species

The species we report as $dIbR_{455}$ may correspond to a species that has been observed by other researchers to occur in solution. The low molar absorptivity of $dIbR_{455}$, along with the blue-shifted λ_{max}, lend support to the hypothesis that it is related to the 450 nm absorbing species reported by Fischer et al. (1981) and Maeda et al. (1980), which was obtained by titrating pink membrane to pH > 6 in aqueous or hydrated systems (see Fig. 1). Maeda et al. (1980) reported the molar absorptivity of this 450 nm species to be approximately half of that observed for the blue membrane, consistent with our observations for $dIbR_{455}$ in dry PVA films. If $dIbR_{455}$ is, in fact, the same as the 450 nm species reported in these investigations, then the dry PVA environment differs from solution in that both the pink membrane and the 450 nm absorbing species are observable in the same environment.

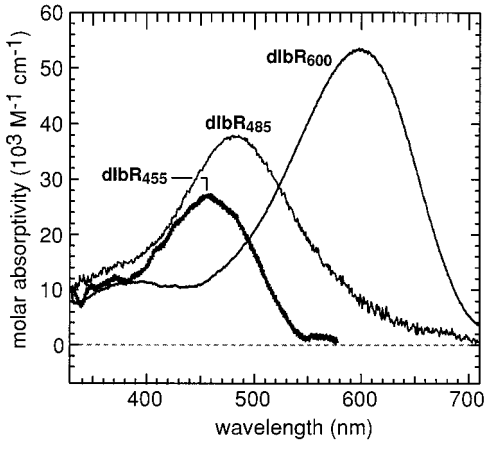

FIGURE 8 The calculated spectrum of $dIbR_{455}$, along with $dIbR_{485}$ and $dIbR_{600}$. The molar extinction coefficient of $dIbR_{455}$ is ~26,000 cm^{-1} M^{-1}, assuming a molar extinction coefficient of 54,760 cm^{-1} M^{-1} for $dIbR_{600}$.

Preliminary photophysical model

The key observations characterizing the $dIbR_{600}/dIbR_{485}/dIbR_{455}$ system in the dry polymer matrix can be summarized as follows: 1) when spectra are acquired under conditions of very dim broadband illumination, photochromic conversion in the film appears to follow $dIbR_{600} \rightarrow dIbR_{455}$; 2) when spectra are acquired under conditions of bright broadband illumination, photochromic conversion appears to follow $dIbR_{600} \rightarrow dIbR_{485}$; 3) when the film is exposed to bright broadband illumination after photoconversion, and spectra are subsequently acquired under conditions of very dim broadband illumination, photochromic conversion appears to follow $dIbR_{600} \rightarrow dIbR_{455}$.

These observations suggest the photophysical model shown in Scheme 1. Under this model, $dIbR_{455}$ is the product of fast thermal decay of $dIbR_{485}$, which is the primary photoproduct of $dIbR_{600}$. Under conditions of sufficiently intense broadband illumination, a quasi-photostationary state is produced with equilibrium shifted from $dIbR_{455}$ toward $dIbR_{485}$. This preliminary model has physical consequences that will be experimentally verifiable. Fast time-resolved spectroscopy of photoconversion of $dIbR_{600}$ should show transient formation of $dIbR_{485}$ followed by fast decay to form $dIbR_{455}$. We note that the value listed for Φ_1 ($< 1.6 \times 10^{-4}$) is based on the measurement of (Liu and Ebrey, 1987b) as providing an upper limit. Our observations indicate that dehydration decreases the quantum efficiency by factors of two or more, in general agreement with previous studies (Chang et al., 1987).

Molecular modeling of the photoisomerization processes

To gain further insight into the photochemical processes of the deionized blue membrane, we carried out MM2 molecular mechanics, MNDO/PM3, and ZINDO/S semiempirical molecular orbital calculations. We had two goals in carrying out the theoretical portion of this research. First, we sought to understand why $dIbR_{600}$ photochemistry selects both 9-*cis* and 13-*cis* photoproducts, whereas native light-adapted bR (bR_{LA}) selects only the 13-*cis* photoproduct.

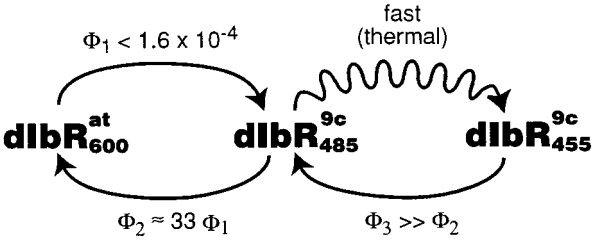

Scheme 1 Apparent photochemistry of deionized blue membrane in dried film.

Second, we sought a molecular model of the two blue-shifted photoproducts, $dIbR_{455}$ and $dIbR_{485}$. Our MNDO/PM3 calculations included the chromophore and all the amino acids within 5 Å of the chromophore (Fig. 9). Our MM2 calculations included the chromophore and all the amino acids within 10 Å of the chromophore. The starting geometry for all calculations was derived from the coordinates obtained by Henderson and co-workers from analysis of electron cryomicroscopy diffraction data (Grigorieff et al., 1996), and an additional shell of residues was added (but not minimized) to constrain the radial expansion of the outer shell of the protein residues. All calculations minimized all internal coordinates relative to a selected fixed internal coordinate assuming a fixed protein backbone. The results of the MM2 calculations are presented in Tables 1–3, with calculations reported for three different binding site counterion environments ($\{ASP_{85}^-, ASP_{212}^-\}$, $\{ASP_{85}H, ASP_{212}^-\}$, $\{ASP_{85}H, ASP_{212}H\}$). Adiabatic MNDO/PM3 potential energy surfaces were calculated for torsional motion about the $C_{9=10}$ and $C_{13=14}$ dihedral angles for these same environments, and the results are shown in Fig. 10. The adiabatic energies for a given surface were fit to a 49-term Fourier series,

$$E(x) = a_0 + \sum_{i=1}^{24} [a_i \cos(x\pi) + b_i \sin(x\pi)] \qquad (3)$$

which compensates for the fact that there is a slight mismatch in energies depending upon the direction in which the surface was generated. Thus, the actual data points and the Fourier surfaces do not rigorously coincide at the edges. We have also adjusted the a_0 values for the excited-state calculations so that each of the excited-state surfaces is isoenergetic at 180° with an arbitrary excitation energy of 30 kcal mol^{-1} for the 13-*cis* set and 40 kcal mol^{-1} for the 9-*cis* set.

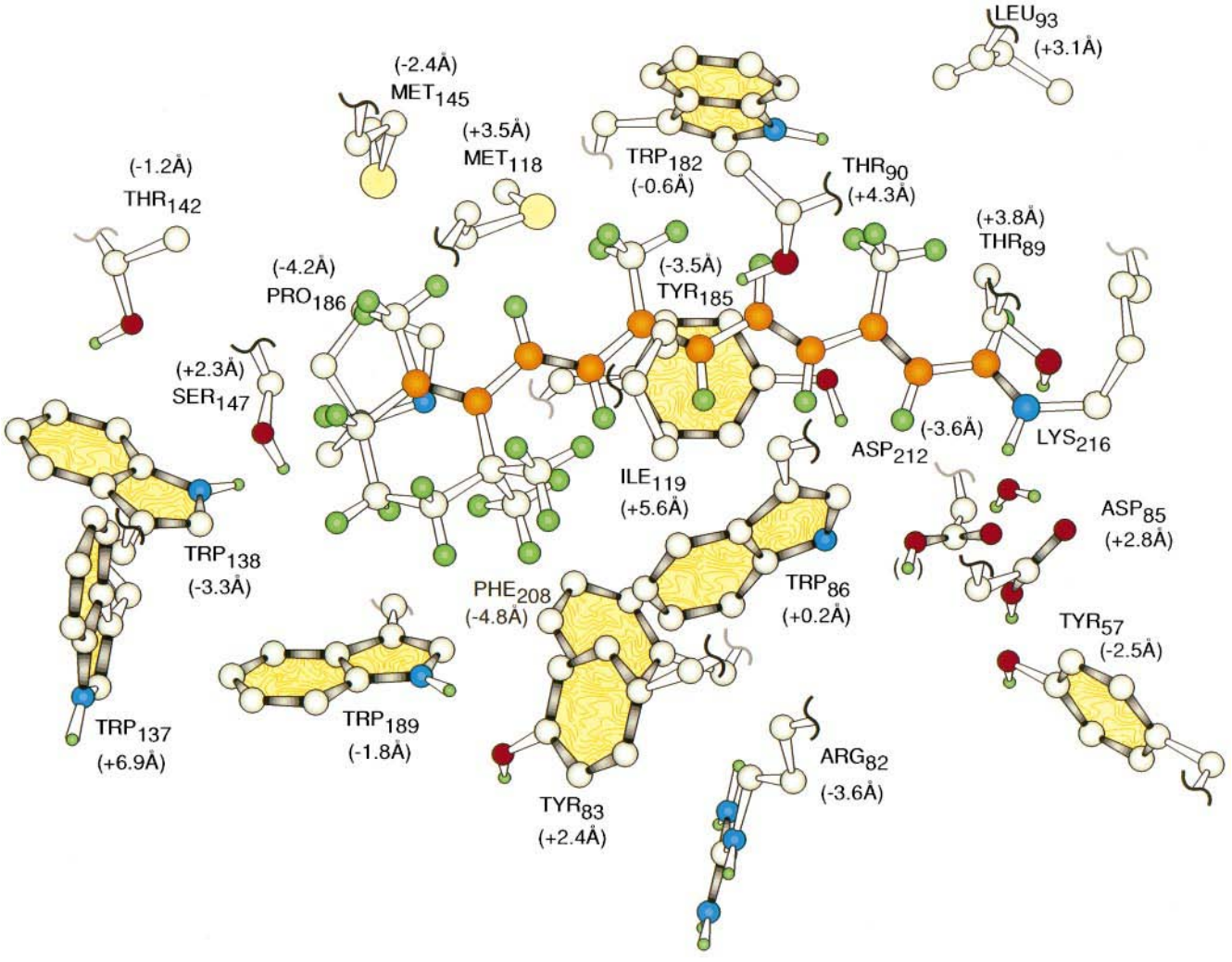

FIGURE 9 A view of the chromophore binding site of $dIbR_{600}$ along with the nearby amino acid residues included in the MNDO/PM3 molecular orbital simulations. The ASP_{212} residue is shown protonated, but we also investigated some models of the binding site where this residue was unprotonated (see text). The MM2 calculations included an additional shell of residues around the chromophore. The numbers shown in parentheses give the center of mass displacements above (positive, out of the paper) and below (negative, into the paper) the chromophore polyene chain (in the plane of the paper).

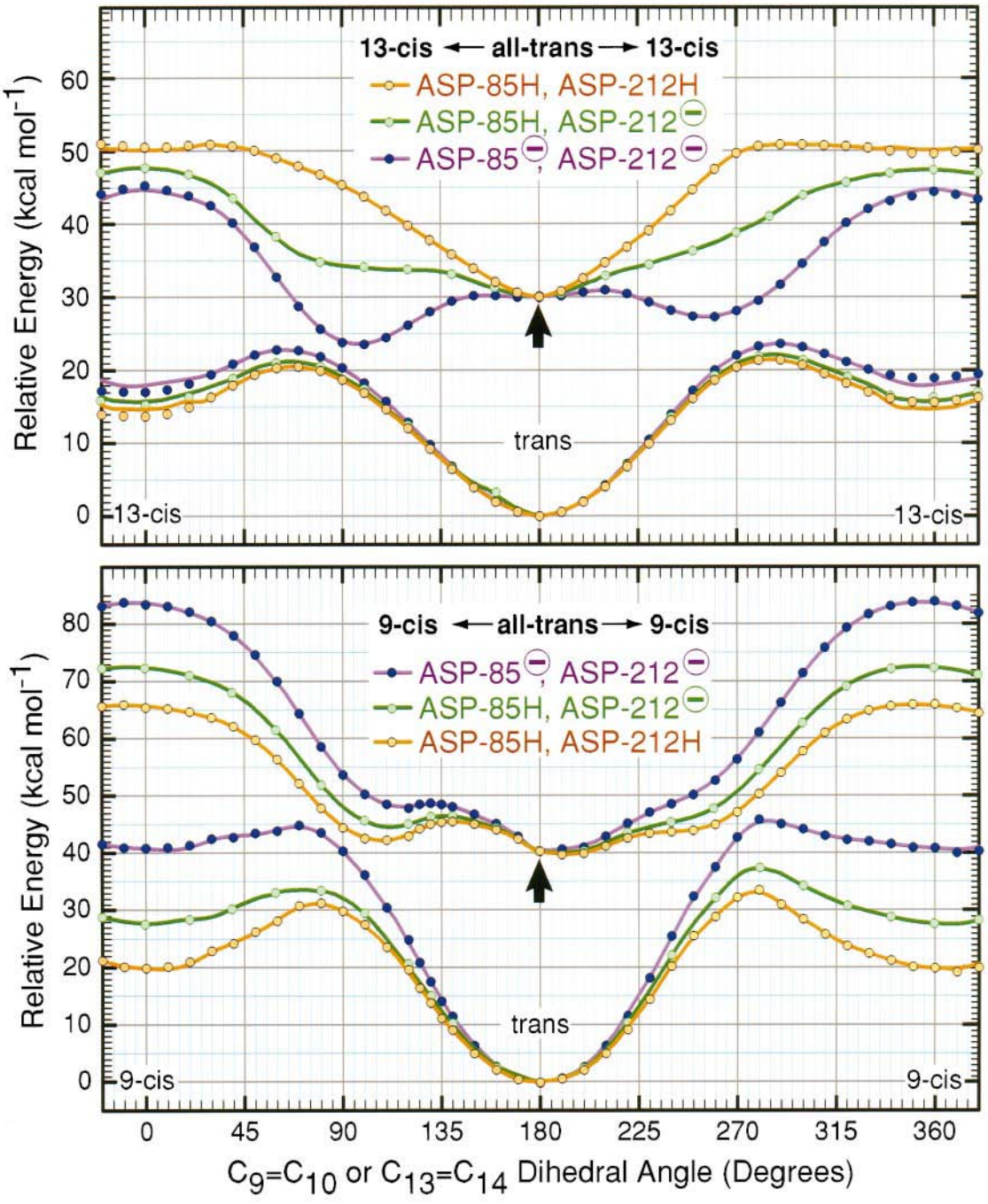

FIGURE 10 Adiabatic ground and excited-state potential energy surfaces for the protonated Schiff base chromophore shown in Fig. 9 as a function of protonation states of the two nearby ASP residues (ASP_{85} and ASP_{212}) for dihedral distortion about the $C_9{=}C_{10}$ and $C_{13}{=}C_{14}$ double bonds. The ground state potentials were generated using MNDO/PM3 molecular orbital theory and the excited-state potentials were calculated using the ground-state geometry as a starting point, but included full single and double CI with the homo − 4 through lumo + 4 chromophore π molecular orbitals. All the ground-state potential energy surfaces were adjusted relative to the all-*trans* (180°) energy. The excited-state potential energy surfaces were adjusted relative to the levels indicated by the two arrows.

This approach enhances comparison, and no useful information is lost, because we used single and double CI in calculating the excited-state surface but no CI in generating the ground-state surface. Thus, the calculated excitation energies were uniformly too low, and only relative differences along a given surface have physical meaning.

In a majority of the following discussion, we make the assumption that ASP_{85} and ASP_{212} are both unprotonated in bR_{LA} (Table 1) and that ASP_{85} is solely protonated in $dIbR_{600}$ (Table 2). There is ample evidence to support the protonation of ASP_{85} in the blue membrane (Metz et al., 1992; Ebrey, 1993). The state of ASP_{212} in the blue mem-

TABLE 1 MM2 analysis of binding site with ASP_{85} and ASP_{212} unprotonated

Component*	all-*trans*[#]	9-*cis*[§]	11-*cis*[¶]	13C, 15A[‖]	13C, 15S**
Stretch	24.9131	24.7988	25.0289	24.8541	24.6609
Bend	117.5695	122.3140	119.2877	117.3618	117.2210
Stretch-Bend	−0.9910	−0.9998	−0.9632	−1.0072	−0.9456
Torsion	−54.6162	−41.2164	−49.4395	−41.8804	−55.6137
Non-1,4 VDW	−105.5952	−89.6723	−95.7670	−105.8180	−101.2293
1,4 VDW	86.6928	85.6145	85.4180	84.6967	85.1792
Charge/Charge	−148.0132	−144.4040	−131.5797	−140.9949	−155.4522
Charge/Dipole	−8.3143	−5.0061	−9.3643	−10.0144	−7.7993
Dipole/Dipole	6.5172	7.6708	6.7188	6.2479	6.2386
Total	−81.8372	−40.9005	−50.6604	−66.5543	−87.7403
$\Delta\Delta E$[##]	0.0	40.9367	31.1768	15.2829	−5.9031

This binding site represents one possible model of the binding site of light-adapted bacteriorhodopsin (see text).
*Energy component of the MM2 calculation. All energies are in kcal mol^{-1} (multiply by 4.184 to convert to kJ mol^{-1}).
[#]The system has been minimized for the all-*trans* protonated Schiff base chromophore.
[§]The system has been minimized for the 9-*cis* protonated Schiff base chromophore.
[¶]The system has been minimized for the 11-*cis*, 15-*anti* protonated Schiff base chromophore.
[‖]The system has been minimized for the 13-*cis*, 15-*anti* protonated Schiff base chromophore, the geometry of the chromophore in the K, L, and M intermediates of bR.
**The system has been minimized for the 13-*cis*, 15-*syn* protonated Schiff base chromophore, the geometry of the 13-*cis* dark-adapted species.
[##]Relative adiabatic energy of binding site relative to that occupied by the all-*trans* protonated Schiff base chromophore.

brane is less certain. Based on pK_a values (Sampogna and Honig, 1994), one would anticipate that both ASP_{85} and ASP_{212} would become protonated at pH levels below 2. In contrast, the solid-state NMR experiments of Metz et al. suggest that ASP_{212} remains unprotonated, at least in the deionized blue membrane (Metz et al., 1992). The spectroscopic and photochemical similarities between the acid blue and deionized blue states, however, suggest the chromophore in both species has a similar, if not identical, counterion environment. We conclude that it is likely that ASP_{212} is unprotonated, but for the purposes of comparison, calculations have been carried out for two counterion environments: $\{ASP_{85}H + ASP_{212}^{-}\}$ and $\{ASP_{85}H + ASP_{212}H\}$ (see below). (We will ultimately conclude that our theoretical studies are significantly more consistent with the assumption that ASP_{212} is unprotonated in the blue membrane.)

The MM2 calculations indicate that the relative stability of the all-*trans*, 9-*cis*, 11-*cis*, and 13-*cis* protonated Schiff base chromophores are highly sensitive to the protonation states of the nearby ASP residues. The bR_{LA} binding site simulations (Table 1) predict energies in the following order: 13-*cis*, 15-*syn* < all-*trans* ≪ 13-*cis* ≪ 11-*cis* < 9-*cis* (where a 15-*anti* conformation is assumed in all calculations unless specified otherwise). Protonation of ASP_{85} dramatically changes the electrostatic environment of the binding site, and the isomer energies are changed to the following relative ordering: all-*trans* < 13-*cis*, 15-*syn* < 13-*cis* < 11-*cis* < 9-*cis*. Protonation of both ASP_{85} and ASP_{212} raises the energy of the system, but the relative ordering remains the same. However, with each progressive increase in protonation degree, the energetic differences become smaller, but the 9-*cis* isomer is always the least

TABLE 2 MM2 analysis of binding site with ASP_{85} protonated and ASP_{212} unprotonated

Component	all-*trans*	9-*cis*	11-*cis*	13C, 15A	13C, 15S
Stretch	24.4054	25.0090	25.6840	25.7070	25.6502
Bend	118.7355	122.0327	118.2680	117.9548	116.3223
Stretch-Bend	−1.0958	−1.0242	−0.9704	−1.0835	−1.1047
Torsion	−53.7177	−48.9412	−54.4935	−44.9186	−58.0382
Non-1,4 VDW	−106.8032	−91.8702	−97.3334	−104.8985	−104.5599
1,4 VDW	86.1668	86.0501	84.4898	84.9210	86.0014
Charge/Charge	−135.7575	−135.0941	−123.8151	−136.2830	−138.5856
Charge/Dipole	−10.4040	−7.0535	−5.8267	−6.0372	−1.4861
Dipole/Dipole	3.2224	6.2509	6.4607	5.7640	5.7021
Total	−75.2481	−44.6405	−47.5366	−58.8742	−70.0985
$\Delta\Delta E$	0.0	30.6076	27.7115	16.3739	5.1496

This binding site represents a realistic model of the deionized blue membrane as well as the acid blue membrane (see text).
*See Table 1 for explanation of data.

TABLE 3 MM2 analysis of binding site with ASP_{85} and ASP_{212} protonated

Component	all-*trans*	9-*cis*	11-*cis*	13C, 15A	13C, 15S
Stretch	24.3077	24.3143	24.5094	24.6240	24.8578
Bend	115.8578	115.3891	118.0236	117.1475	116.8552
Stretch-Bend	−1.0644	−1.0625	−1.0421	−1.0689	−1.2066
Torsion	−64.8652	−59.9161	−58.1871	−56.0177	−62.3608
Non-1,4 VDW	−125.0133	−111.9661	−117.8466	−121.4802	−115.3282
1,4 VDW	83.8504	84.7276	83.9775	83.8681	84.5901
Charge/Charge	−42.0308	−42.7714	−42.5107	−42.3171	−41.4209
Charge/Dipole	0.9274	1.0317	1.0527	0.9526	−2.3833
Dipole/Dipole	5.6268	5.9472	5.9443	5.8334	6.4414
Total	−2.4036	15.6938	13.9209	11.5418	10.0448
$\Delta\Delta E$	0.0	18.0974	16.3245	13.9454	12.4484

This binding site represents an alternative model of the deionized blue membrane as well as the acid blue membrane (see text).
*See Table 1 for explanation of data.

stable and the all-*trans* isomer is always the most stable of the 15-*anti* species. Thus, the MM2 calculations do not provide a satisfactory explanation of the formation of the long-lived 9-*cis* pink species upon irradiation of the blue membrane.

The ratio of all-*trans* to 13-*cis*, 15-*syn* in dark-adapted bR is ~40%:60%, but lowering the pH to 2 or less to produce the acid blue membrane stabilizes the former to yield a ratio of all-*trans* to 13-*cis*, 15-*syn* isomers of ~60%:40% (see Fig. 1 of Koyama et al., 1993). The MM2 simulations predict the 13-*cis*, 15-*syn* species is the most stable in bR_{DA} (Table 1) and the all-*trans* isomer is the most stable in the blue membrane (Table 2). While the simulations overestimate the energetic differences, analysis of the MM2 energy components suggests that the 13-*cis*, 15-*syn* species is destabilized upon protonation of ASP_{85} primarily through the loss of charge/dipole interactions between the chromophore and this residue. From a molecular standpoint, the MM2 calculations predict that ionized ASP_{85} stabilizes the 13-*cis*, 15-*syn*-isomer more effectively than the all-*trans* isomer. This observation is in good agreement with the experimental studies of Balashov et al. (1996), who explained the increased fraction of all-*trans* isomer in the blue membrane in terms of different pK_a values of ASP_{85} in blue versus purple membrane. The different pK_a values are due presumably to different energies of interaction of ionized ASP_{85} with 13-*cis*, 15-*syn* versus all-*trans* protonated Schiff base isomers (Balashov et al., 1996).

Analysis of the MM2 energy components indicates that torsional distortion and non-1,4-van der Waals interactions are the key nonelectrostatic determinants determining the relative stability of the isomers. (We will demonstrate below that $dIbR_{455}$ may represent a torsionally distorted 9-*cis* species derived from relaxation of $dIbR_{485}$.) The MM2 calculations also indicate the importance of charge/charge and charge/dipole interactions in comparative electrostatic stabilization of the various isomers. The MM2 calculations do not provide a perspective on why the blue membrane yields a long-lived 9-*cis* photoproduct. To understand this phenomenon requires analysis of the excited state potential energy surfaces (see below).

Analysis of the excited-state potential energy surfaces shown in Fig. 10 provides a perspective on the photochemical selectivity of the protein binding sites of bR_{LA} and dIbR. The excited-state potential surfaces for all-*trans* → 13-*cis* versus all-*trans* → 9-*cis* in bR_{LA} (ASP^{-}_{85} and ASP^{-}_{212}) clearly favor formation of the 13-*cis* isomer. Upon excitation of the all-*trans* chromophore, formation of the 13-*cis* isomer can proceed along a nearly barrierless surface (Fig. 10, *top*) while formation of the 9-*cis* isomer requires that a barrier of ~9 kcal mol^{-1} be surmounted. At ambient temperature, unimolecular reaction rate theory predicts that the 13-*cis* isomer will be favored by a factor of 10^6 over formation of the 9-*cis* isomer. Protonation of ASP_{85}, however, increases the all-*trans* → 13-*cis* excited state barrier to ~4 kcal mol^{-1}, but decreases the all-*trans* → 9-*cis* excited state barrier to ~6 kcal mol^{-1}. Unimolecular reaction rate theory and the assumption of identical prefactors suggest that the rate of forming the 13-*cis* isomer is still favored by a factor of ~30. If we assume further that the relative quantum yields are proportional to these rates, then if $\Phi_{at\rightarrow 13} \approx 0.1$ (Ohtani et al., 1986) we predict $\Phi_{at\rightarrow 9} \approx 0.003$ in the blue membrane. Our quantitative prediction is more than one order of magnitude too large (see Scheme 1), but given the approximations inherent in the calculation, satisfactory. If we make the assumption that both ASP_{85} and ASP_{212} are protonated, our calculations predict no photochemistry along the all-*trans* → 13-*cis* torsional coordinate, because the excited state barrier is so high (Fig. 10). Thus, our calculations, when examined in light of the experimental studies of Ohtani et al. (1986), support the assumption that ASP_{212} remains unprotonated in the deionized blue membrane (Metz et al., 1992). Additional support for the role of ASP_{85} in enhancing all-*trans* → 9-*cis* photochemistry can be found in the study of the R82A (ARG_{82} to ALA_{82}) mutant, in which the pink membrane is formed at nominal pH (Balashov et al., 1993). The pK_a of ASP85 is increased to 7.2 in R82A (Balashov et al., 1993), which allows for the protonation of this residue, and the photochemical formation of a pink membrane species, at a higher pH than in the native protein.

The relative excited-state barriers are very sensitive to the CI basis set, and the absolute barriers are particularly sensitive to the amount of double CI. An attempt to correlate the CI coefficients with the excited state surfaces provided little perspective on the relative barriers. All of the orthogonal or nearly orthogonal configurations were stabilized by doubly excited configurations and produced large dipolar charge separations across the twisted double bond (see, for example, Salem and Bruckmann, 1975; Birge and Hubbard, 1980; Tallent et al., 1992). However, the principal difference between the 13-*cis*oid-orthogonal and the 9-*cis*oid-orthogonal conformations is that the former is stabilized by the presence of negative charge in the ASP_{85}, ASP_{212} region, whereas the latter is destabilized by such charges. Thus, the preferential formation of one isomer over the other is determined in part by the charge redistribution and polarization along the polyene chain during isomerization, and the interaction of such with the one or two negatively charged ASP residues.

Molecular modeling of the $dIbR_{485}$ and $dIbR_{455}$ states

We carried out a series of calculations using MM2, MNDO/PM3, ZINDO/S and MNDO/CI methods to examine potential models of the two blue-shifted states. The 9-*cis* isomer is consistently viewed as the principal long-lived photoproduct of blue membrane photochemistry. However, a small amount of 11-*cis* isomer is also formed (Maeda et al., 1980, 1981) and at certain wavelengths or high pH values, the 11-*cis* isomer is the dominant photoproduct (Koyama et al., 1993). We investigated the theoretical possibility that either $dIbR_{485}$ or $dIbR_{455}$ might represent the 11-*cis* species, and concluded that our theoretical methods are not able to differentiate between 9-*cis* versus 11-*cis* isomers with respect to the spectroscopic or photochemical properties. Although our MM2 calculations suggest the 11-*cis* isomer is slightly more stable than the 9-*cis* isomer in the $ASP_{85}H$, ASP^{-}_{212} binding site (see Table 2), the differences are smaller than the accuracy of the method. We anticipate that $dIbR_{485}$ and $dIbR_{455}$ are likely the same double-bond isomer because $dIbR_{485}$ apparently undergoes a rapid thermal reaction to form $dIbR_{455}$. The MNDO/PM3 calculations predict barriers ranging from 15 to 40 kcal mol^{-1} for ground state isomerizations involving the 9═10, 11═12, and 13═14 double bonds. Thus, we conclude that both $dIbR_{485}$ and $dIbR_{455}$ share the same double-bond isomeric composition. Based on the experimental data of Koyama et al. at low pH and red excitation wavelengths, we conclude that both of the long-lived intermediates we observe have 9-*cis* geometries (Koyama et al., 1993).

There are at least two molecular scenarios that might occur whereby $dIbR_{485}$ would thermally decay to yield a blue-shifted species. The first scenario we investigated is a deprotonation of an amino acid in the C_{10}—C_{11}═C_{12}—C_{13}═C_{14}—C_{15}═N region of the chromophore, which will induce a blue-shift in the absorption spectrum. If we assume for the moment that ASP_{212} is protonated, then deprotonation of this amino acid could be responsible. The ZINDO/S calculations shown in Fig. 11 indicate that deprotonation of ASP_{212} induces a shift in the 9-*cis* chromophore from λ_{max} = 495 nm to λ_{max} = 410 nm. This shift is much larger than observed, but given the approximations inherent in our use of semiempirical methods, the agreement is acceptable. Less acceptable is that the significant decrease in the oscillator strength observed accompanying the $dIbR_{485}$ to $dIbR_{455}$ transformation (see Fig. 8) is not reproduced by the calculation (Fig. 11). Indeed, test calculations involving the deprotonation of any nearby ASP or TYR residues were not capable of simultaneously reproducing a blue shift and a decrease in the oscillator strength of the λ_{max} band. We conclude that deprotonation of a nearby residue is unlikely to be the dominant molecular event, although it might well be coupled to a conformational change of the chromophore (see below).

An alternative model of the $dIbR_{455}$ state is shown in Figs. 12 and 13. This model is characterized by a significant dihedral distortion of the C_{10}—C_{11} single bond. We obtain this geometry when we include double CI in the MNDO/PM3 ground state calculations and carry out simulated annealing of the 9-*cis* $ASP_{85}H$ binding site. If double CI is not included, the single-bond distortions are more equally distributed, but a majority of the distortion is still concentrated in the C_{10}—C_{11} single bond. The molecular origin of

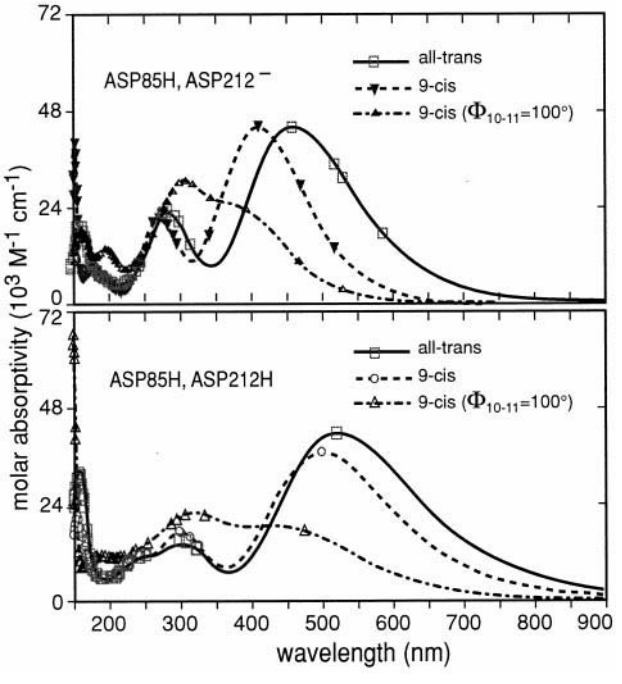

FIGURE 11 ZINDO/S theoretical simulations of the absorption spectra of the all-*trans*, 9-*cis*, and 9-*cis*, 10-s-distorted ($\Phi_{10—11}$ = 100°) chromophores in two models of the deionized bR binding site. The spectra in the top insert were calculated assuming ASP_{85} is protonated and ASP_{212} is deprotonated, while the spectra in the bottom insert were calculated assuming the above two ASP residues are both protonated.

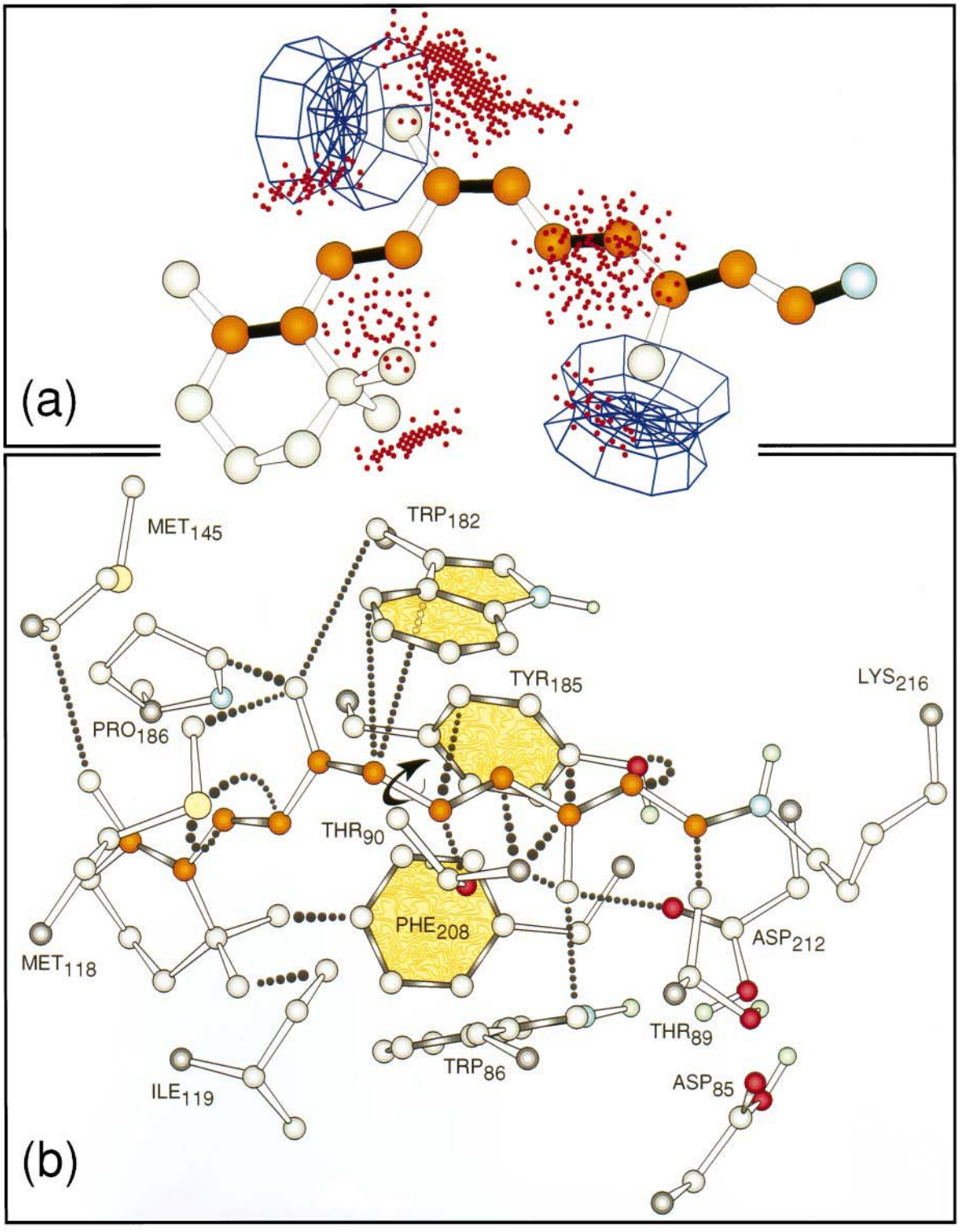

FIGURE 12 The chromophore binding site of bacteriorhodopsin is not designed to accommodate 9-*cis* retinal, and incorporation of the 9-*cis* chromophore into the binding site introduces significant repulsive interactions associated with the two polyene methyl groups as shown in (*a*). The directionality of the interatomic interactions are indicated using the wireframe potential maps, and the intensity of the interactions are indicated by the number of dots in the top figure. The bottom figure shows the principal nearest neighbor interactions that drive the 9-*cis* chromophore to nonplanarity around the C_{10}—C_{11} bond.

this distortion is examined in Fig. 12, where the principal chromophore-protein interactions responsible for driving this distortion are indicated. The key feature of this model is that the C_{10}—C_{11} single-bond distortion induces not only a blue shift, but also a significant decrease in the oscillator strength of the λ_{max} absorption band (compare Figs. 8 and

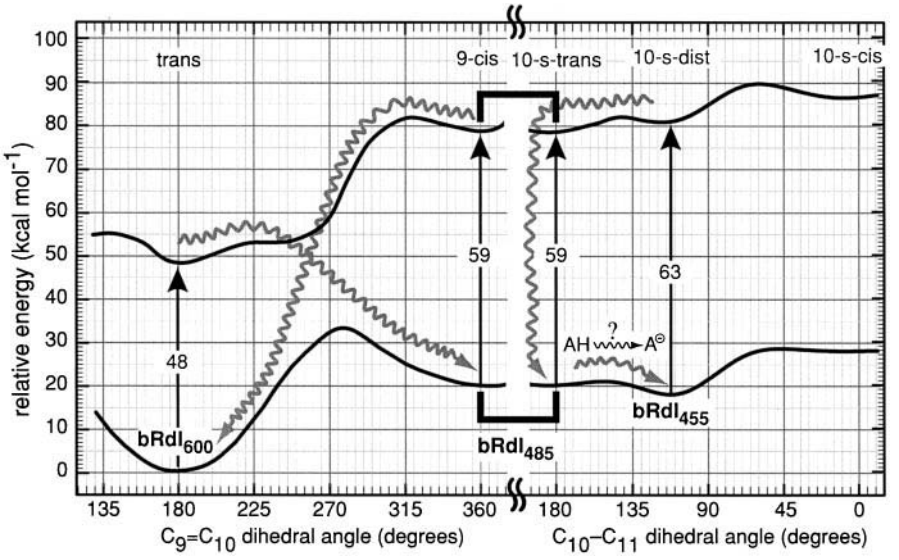

FIGURE 13 A schematic diagram of the ground- and excited-state potential energy surfaces associated with the thermal and photophysical properties of the deionized blue membrane of bacteriorhodopsin in dried thin films. Dark arrows indicate light absorption (with the transition energy indicated in kcal mol^{-1}) and thermal radiationless relaxation or decay processes are indicated with gray zig-zag arrows. Note that the two central minima in the diagram corresponding to $\Phi_{9=10} = 360°$ (left lower surface) and $\Phi_{10-11} = 180°$ (right lower surface) define the properties of a single intermediate, dIbR$_{485}$. This intermediate thermally decays to form dIbR$_{455}$ via distortion about C$_{10}$—C$_{11}$. The latter relaxation may be accompanied by a deprotonation of a nearby ionic residue [dIbR$_{485}$(AH) → dIbR$_{455}$(A$^-$)].

11). We do not suggest that the dIbR$_{455}$ has a C$_{10}$—C$_{11}$ single bond distorted to the precise extent investigated in Fig. 11; rather, we propose that dIbR$_{455}$ has a range of C$_{10}$—C$_{11}$ single-bond distortions (Fig. 13) that yields inhomogeneous broadening in the electronic spectrum. This model of dIbR$_{455}$ may be the dried film analog of the 450-nm state observed when the pH of an acid pink membrane solution is adjusted toward neutrality. In this case, we observe a 50-nm shift (Fig. 1), which is in better agreement with the calculated shift predicted for deprotonation of ASP$_{212}$ (Fig. 11). We note that analysis of the ZINDO/S calculations shown in Fig. 11 suggests that a deprotonated ASP$_{212}$ fits the electronic spectral data of dIbR$_{485}$ and dIbR$_{455}$, while a protonated ASP$_{212}$ fits the dIbR$_{600}$ spectrum best. If dIbR$_{455}$ (Fig. 13) and BR450 (Fig. 1) are analogous, we anticipate that formation of the former may also be accompanied by a deprotonation of a nearby ionic residue [i.e., dIbR$_{485}$(AH) → dIbR$_{455}$(A$^-$)]. This latter assumption would help explain the observed pH effect.

COMMENTS AND CONCLUSIONS

We have demonstrated the successful fabrication of dried blue membrane/PVA films. These films show modest potential for device applications, because once formed and sealed, they demonstrate excellent thermal and photochemical stability. However, the quantum efficiencies for photochromic applications are too low for most applications. Reversible photoconversion to the pink membrane occurs in these films under conditions of intense 647-nm laser irradiation. Because of the low quantum efficiency of the dIbR$_{600}$ → dIbR$_{485}$ photoconversion, high power densities are required to achieve appreciable conversion on a time scale of seconds. Under these conditions, localized heating of the film is likely to cause protein denaturation unless precautions such as interval illumination are taken. We have provided evidence for the existence of a second photoproduct having a very low extinction coefficient and a λ_{max} blue-shifted with respect to the pink membrane. The properties of this species are consistent with those reported for the 450-nm absorbing species reported in previous studies of aqueous systems. Whereas these previous studies produced the 450-nm species by titration of the pink membrane to pH > 6, both may be photoproducts of the blue membrane in dried PVA films. We propose a preliminary photophysical model of this system in which dIbR$_{455}$ is the product of fast thermal decay of dIbR$_{485}$, which is the initial photoproduct of dIbR$_{600}$. Molecular modeling of the binding site indicates that charge/charge and charge/dipole interactions introduced by the protonation of ASP$_{85}$ are responsible for stabilizing preferentially the all-*trans* → 9-*cis* photochemistry observed in the blue membrane. The molecular orbital calculations suggest that dIbR$_{455}$ may be a 9-*cis*, 10-s-distorted species that partially divides the chromophore into two conjugated segments with a concomitant blue shift and decreased oscillator strength of the λ_{max} absorption band. The formation of dIbR$_{455}$ may be accompanied by a deprotonation of a nearby ionic residue [dIbR$_{485}$(AH) → dIbR$_{455}$(A$^-$)], and is driven by interactions between the C$_9$ and C$_{13}$ chromophore methyl groups and protein residues.

Our theoretical calculations also provide some interesting perspectives on recent femtosecond studies of the primary photochemical events in bacteriorhodopsin (Haran et al., 1996; Hasson et al., 1996) and blue membrane-like mutants (Song et al., 1993). The studies by Haran et al. (1996) and Hasson et al. (1996) indicate that the Franck-Condon region of the 13-*trans* → 13-*cis* surface does not provide a steep dynamic decay route. Our MNDO-PSDCI excited-state surface can be analyzed more easily by reference to Fig. 14, which shows an expanded view of the Franck-Condon region plotted in Fig. 10. The key observation is the presence of a small, but nonnegligible, barrier in the adiabatic surface for motion in both dihedral directions. Our calculations lack

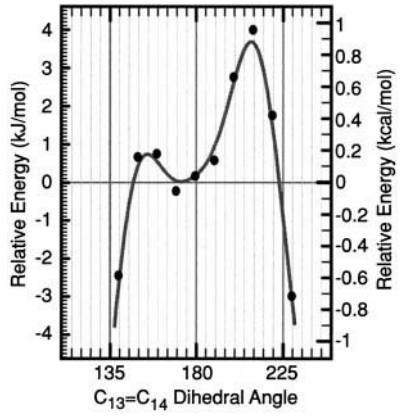

FIGURE 14 Franck-Condon region of the adiabatic S_1 surface associated with the 13-*trans* → 13-*cis* torsional coordinate of light-adapted bacteriorhodopsin.

sufficient rigor to view this surface as a quantitative model, but our results do suggest that there are a number of torsional vibronic levels localized within the Franck-Condon region, and that the excited state might well remain within this region for a short time before moving along the 13-*trans* → 13-*cis* excited state torsional surface. We note further that the molecule would likely experience effective barriers larger than those predicted via adiabatic mapping; but in the absence of dynamic simulations, no quantitative prediction can be made. It is sufficient to note for the present purposes that our MNDO-PSDCI calculations are fully consistent with the observation of a metastable Franck-Condon excited state that evolves into a dynamic system after 0.1–0.2 ps. We also note that these surfaces provide a perspective on the interesting studies of Song et al. (1993) on the decay of the excited state absorption as a function of binding site mutation; this study shows that the excited state of native bR lives for ~500 fs, and displays single exponential decay. In contrast, the blue membrane-like mutant D85N (λ_{max} = 604 nm) has a much longer excited-state lifetime with a multicomponent decay of 35% fast (2 ps) and 65% slow (10 ps). The dramatic difference no doubt reflects the change from a nearly barrierless surface for 13-*trans* → 13-*cis* (Fig. 14) to a surface with multiple decay pathways (including both 13-*trans* → 13-*cis* and 9-*trans* → 9-*cis*), all of which have barriers (Fig. 10).

This work was supported in part by National Institutes of Health Grant GM-34548, National Science Foundation Grant CHE-96-0022N, the W. M. Keck Foundation, and National Science Foundation Postdoctoral Fellowship in Chemistry CHE-95-04697 (to C.H.M.).

REFERENCES

Balashov, S., R. Govindjee, M. Kono, E. Imasheva, E. Lukashev, T. Ebrey, R. Crouch, D. Menick, and Y. Feng. 1993. Effect of the arginine-82 to alanine mutation in bacteriorhodopsin on dark adaptation, proton release, and the photochemical cycle. *Biochemistry.* 32:10331–10343.

Balashov, S. P., E. S. Imasheva, R. Govindjee, M. Sheves, and T. G. Ebrey. 1996. Evidence that aspartate-85 has a higher pKa in all-*trans* than in 13-*cis* bacteriorhodopsin. *Biophys. J.* 71:1973–1984.

Birge, R. R. 1990a. Nature of the primary photochemical events in rhodopsin and bacteriorhodopsin. *Biochim. Biophys. Acta.* 1016:293–327.

Birge, R. R. 1990b. Photophysics and molecular electronic applications of the rhodopsins. *Annu. Rev. Phys. Chem.* 41:683–733.

Birge, R. R. 1994. Bacteriorhodopsin, a nonlinear proton pump. *Nature.* 371:659–660.

Birge, R. R., D. S. K. Govender, K. C. Izgi, and E. H. L. Tan. 1996. Role of calcium in the proton pump of bacteriorhodopsin. Microwave evidence for a cation-gated mechanism. *J. Phys. Chem.* 100:9990–10004.

Birge, R. R., and L. M. Hubbard. 1980. Molecular dynamics of *cis-trans* isomerization in rhodopsin. *J. Am. Chem. Soc.* 102:2195–2204.

Birge, R. R., B. Parsons, Q. W. Song, and J. R. Tallent. 1997. Protein-based three-dimensional memories and associative processors. *In* Molecular Electronics. Blackweel Science Ltd., Oxford. 439–471.

Buckert, U., and N. L. Allinger. 1982. Molecular Mechanics. American Chemical Society, Washington, D.C.

Chang, C.-H., J. G. Chen, R. Govindjee, and T. Ebrey. 1985. Cation binding by bacteriorhodopsin. *Proc. Natl. Acad. Sci. USA.* 82:396–400.

Chang, C.-H., R. Jonas, R. Govindjee, and T. G. Ebrey. 1988. Regeneration of blue and purple membranes from deionized bleached membranes. *Photochem. Photobiol.* 47:261–265.

Chang, C.-H., R. Jonas, S. Melchiore, R. Govindhee, and T. G. Ebrey. 1986. Mechanism and role of divalent cation binding of bacteriorhodopsin. *Biophys. J.* 49:731–739.

Chang, C.-H., S. Y. Liu, R. Jonas, and R. Govindjee. 1987. The pink membrane: the stable photoproduct of deionized purple membrane. *Biophys. J.* 52:617–623.

Chronister, E. L., and M. M. El-Sayed. 1987. Time-resolved resonance Raman spectra of the photocycle intermediates of acid and deionized bacteriorhodopsin. *Photochem. Photobiol.* 45:507–513.

Chung-Ho, C., R. Jonas, T. G. Ebrey, M. Hong, and L. Eisenstein. 1987. Protonation changes in the interconversions of the pink membrane, blue membrane and purple membrane. *In* Biophysical Studies of Retinal Proteins. University of Illinois Press. 156–166.

Corcoran, T. C., K. Z. Ismail, and M. A. El-Sayed. 1987. Evidence for the involvement of more than one metal cation in the Schiff base deprotonation process during the photocycle of bacteriorhodopsin. *Proc. Natl. Acad. Sci. USA.* 84:4094–4098.

Curtis, K., and D. Psaltis. 1992. Recording of multiple holograms in photopolymer films. *Appl. Opt.* 31:7425–7428.

Dewar, M. J. S., and W. Thiel. 1977. Ground states of molecules. 38. The MNDO method. Approximations and parameters. *J. Am. Chem. Soc.* 99:4899.

Dudek, M. J., and J. W. Ponder. 1995. Accurate modeling of the intramolecular electrostatic energy of proteins. *J. Comput. Chem.* 16:791–816.

Duñach, M., M. Seigneuret, J.-L. Riguad, and E. Padrós. 1988. Influence of cations on the blue to purple transition of bacteriorhodopsin. *J. Biol. Chem.* 263:17378–17384.

Ebrey, T. G. 1993. Light energy transduction in bacteriorhodopsin. *In* Thermodynamics of Membrane Receptors and Channels. CRC Press, Boca Raton, FL. 353–387.

El-Sayed, M. A. 1992. On the molecular mechanisms of the solar to electric energy conversion by the other photosynthetic system in nature, bacteriorhodopsin. *Accts. Chem. Res.* 25:279–286.

El-Sayed, M. A., D. Yang, S.-K. Yoo, and N. Shang. 1995. The effect of different metal cation binding on the proton pumping in bacteriorhodopsin. *Israel J. Chem.* 35:465–474.

Fischer, U. C., P. Towner, and D. Oesterheldt. 1981. Light induced isomerization, at acidic pH, initiates hydrolysis of bacteriorhodopsin to bacterio-opsin and 9-*cis*-retinal. *Photochem. Photobiol.* 33:529–537.

Grigorieff, N., T. A. Ceska, K. H. Downing, J. M. Baldwin, and R. Henderson. 1996. Electron-crystallographic refinement of the structure of bacteriorhodopsin. *J. Mol. Biol.* 259:393–421.

Gross, R. B., A. T. Todorov, and R. R. Birge. 1995. The wavelength-dependent refractive index change associated with the blue to pink membrane photochemical conversion in bacteriorhodopsin. *In* Applications of Photonic Technology. Plenum Press, New York. 115–121.

Gu, C., J. Hong, I. McMichael, R. Saxena, and F. Mok. 1992. Cross-talk-limited storage capacity of volume holographic memory. *J. Opt. Soc. Am.* A9:1978–1983.

Hampp, N., A. Popp, C. Bräuchle, and D. Oesterhelt. 1992. Diffraction efficiency of bacteriorhodopsin films for holography containing bacteriorhodopsin wildtype BRwt and its variants BR_{D85E} and BR_{D96N}. *J. Phys. Chem.* 96:4679–4685.

Haran, G., K. Wynne, A. Xie, Q. He, M. Chance, and R. M. Hochstrasse. 1996. Excited state dynamics of bacteriorhodopsin revealed by transient stimulated emission spectra. *Chem. Phys. Lett.* 261:389–395.

Hasson, K. C., F. Gai, and P. A. Anfinrud. 1996. The photoisomerization of retinal in bacteriorhodopsin: experimental evidence for a three-state model. *Proc. Natl. Acad. Sci. USA.* 93:15124–15129.

Heanue, J. F., M. C. Bashaw, and L. Hesselink. 1994. Volume holographic storage and retrieval of digital data. *Science.* 265:749–752.

Henderson, R., J. M. Baldwin, T. A. Ceska, F. Zemlin, E. Beckmann, and K. H. Downing. 1990. Model for the structure of bacteriorhodopsin based on high-resolution electron cryo-microscopy. *J. Mol. Biol.* 213: 899–929.

Heyn, M. P., C. Dudda, H. Otto, F. Seiff, and I. Wallat. 1989. The purple to blue transition of bacteriorhodopsin is accompanied by a loss of the hexagonal lattice and a conformational change. *Biochemistry.* 28: 9166–9172.

Jonas, R., and T. G. Ebrey. 1991. Binding of a single divalent cation directly correlates with the blue-to-purple transition in bacteriorhodopsin. *Proc. Natl. Acad. Sci. USA.* 88:149–153.

Kamo, N., M. Yoshimoto, Y. Kobatake, and S. Itoh. 1987. Formation of blue membrane of bacteriorhodopsin by addition of tetrakis(4-fluorophenyl)boron, an hydrophobic anion. *Biochim. Biophys. Acta.* 904:179–186.

Kimura, Y., A. Ikegami, and W. Stoeckenius. 1984. Salt and pH-dependent changes of the purple membrane absorption spectrum. Evidence for changes in conformation of the protein. *Photochem. Photobiol.* 40: 641–646.

Koyama, Y., H. Nakasu, Y. Mukai, and F. Tokunaga. 1993. Isomerization of the retinylidene chromophore of bacteriorhodopsin in light adaptation: intrinsic isomerization of the chromophore and its control by the apo-protein. *Photochem. Photobiol.* 57:732–738.

Lanyi, J. K. 1995. Bacteriorhodopsin as a model for proton pumps. *Nature.* 375:461–463.

Liu, S. Y., and T. G. Ebrey. 1987a. A new method to prepare blue membrane by removing cations from the purple membrane by electrolysis. *Photochem. Photobiol.* 46:557–559.

Liu, S. Y., and T. G. Ebrey. 1987b. The quantum efficiency for the interphotoconversion of the blue and pink forms of purple membrane. *Photochem. Photobiol.* 46:263–267.

Maeda, A., T. Iwasa, and T. Yoshizawa. 1980. Formation of 9-*cis*- and 11-*cis*-retinal pigments from bacteriorhodopsin by irradiating purple membrane in acid. *Biochemistry.* 19:3825.

Maeda, A., I. Tatsuo, and T. Yoshizawa. 1981. Photoreaction of the acidified form of bacteriorhodopsin and its 9-*cis* derivative in purple membrane at low temperatures. *Photochem. Photobiol.* 33:559–565.

Martin, C. H., and R. R. Birge. 1998. Reparameterizing MNDO for excited state calculations using ab initio effective Hamiltonian theory: application to the 2,4-pentadien-1-iminium cation. *J. Phys. Chem. A.* 102: 852–860.

Martin, C. H., Z. P. Chen, and R. R. Birge. 1997. Towards a bacteriorhodopsin-silicon neuromorphic photosensor. *In* Proc. Pacific Symp. Biocomputing. World Scientific, Maui. 268–279.

Mathies, R. A., S. W. Lin, J. B. Ames, and W. T. Pollard. 1991. From femtoseconds to biology: mechanism of bacteriorhodopsin's light-driven proton pump. *Annu. Rev. Biophys. Biophys. Chem.* 20:491–518.

Metz, G., F. Siebert, and M. Engelhard. 1992. ASP_{85} is the only internal aspartic acid that gets protonated in the M intermediate and the purple-to-blue transition of bacteriorhodopsin: a solid-state ^{13}C CP-MAS NMR investigation. *FEBS Lett.* 303:237–241.

Mowery, P. C., R. H. Lozier, Q. Chae, Y. W. Tseng, M. Taylor, and W. Stoeckenius. 1979. Effect of acid pH on the absorption spectra and photoreactions of bacteriorhodopsin. *Biochemistry.* 18:4100–4107.

Oesterhelt, D., and L. Schuhmann. 1974. Reconstitution of bacteriorhodopsin. *FEBS Lett.* 44:262–265.

Oesterhelt, D., and W. Stoeckenius. 1971. Rhodopsin-like protein from the purple membrane of *Halobacterium halobium. Nature (London), New Biol.* 233:149–152.

Oesterhelt, D., and W. Stoeckenius. 1974. Isolation of the cell membrane of *Halobacterium halobium* and its fractionation into red and purple membrane. *Methods Enzymol.* 31:667–678.

Oesterhelt, D., J. Tittor, and E. Bamberg. 1992. A unifying concept for ion translocation by retinal proteins. *J. Bioenerg. Biomembr.* 24:181–191.

Ohtani, H., T. Kobayashi, and J. Iwai. 1986. Picosecond and nanosecond spectroscopies of the photochemical cycles of acidified bacteriorhodopsin. *Biochemistry.* 25:3356–3363.

Pande, C., R. H. Callender, C. H. Chang, and T. G. Ebrey. 1986. Resonance Raman study of the pink membrane photochemically prepared from the deionized blue membrane of *H. Halobium. Biophys. J.* 50:545–549.

Popp, A., M. Wolperdinger, N. Hampp, C. Bräuchle, and D. Oesterhelt. 1993. Photochemical conversion of the O-intermediate to 9-*cis*-retinal-containing products in bacteriorhodopsin films. *Biophys. J.* 65: 1449–1459.

Qiao, Y., and D. Psaltis. 1992. Sampled dynamic holographic memory. *Appl. Opt.* 17:1376–1378.

Renk, G., P. Goletz, R. K. Crouch, C. Chung-Ho, R. Govindjee, and T. G. Ebrey. 1987. A spin-labeled analogue of purple and blue membrane. *In* Biophysical Studies of Retinal Proteins. University of Illinois Press. 80–85.

Renthal, R., and R. Regalado. 1991. Cooperativity of the dehydration blue-shift of bacteriorhodopsin. *Photochem. Photobiol.* 54:931–935.

Salem, S., and P. Bruckmann. 1975. Conversion of a photon to an electrical signal by sudden polarization in the n-retinylidene visual chromophore. *Nature.* 258:526–528.

Sampogna, R. V., and B. Honig. 1994. Environmental effects on the protonation states of active site residues in bacteriorhodopsin. *Biophys. J.* 66:1341–1352.

Song, L., M. A. El-Sayed, and J. K. Lanyi. 1993. Protein catalysis of the retinal subpicosecond photoisomerization in the primary process of bacteriorhodopsin photosynthesis. *Science.* 261:891–894.

Stewart, J. J. P. 1989. Optimization of parameters for semiempirical methods. *J. Comput. Chem.* 10:221–245.

Stoeckenius, W., and R. Bogomolni. 1982. Bacteriorhodopsin and related pigments of Halobacteria. *Annu. Rev. Biochem.* 52:587–616.

Stuart, J. A., B. W. Vought, C. F. Zhang, and R. R. Birge. 1995. The active site of bacteriorhodopsin. Two-photon spectroscopic evidence for a positively charged chromophore binding site mediated by calcium. *Biospectroscopy.* 1:9–28.

Tallent, J. R., E. Q. Hyde, L. A. Findsen, G. C. Fox, and R. R. Birge. 1992. Molecular dynamics of the primary photochemical event in rhodopsin. *J. Am. Chem. Soc.* 114:1581–1592.

Tallent, J., Q. W. Song, Z. Li, J. Stuart, and R. R. Birge. 1996. Effective photochromic nonlinearity of dried blue-membrane bacteriorhodopsin films. *Optics Letters.* 21:1339–1341.

Tittor, J., and D. Oesterhelt. 1990. The quantum yield of bacteriorhodopsin. *FEBS Lett.* 263:269–273.

Toth-Boconadi, R., S. G. Taneva, and L. Keszthelyi. 1989. Angle of retinal of bacteriorhodopsin in blue membrane. *Biophys. J.* 56:281–283.

Tributsch, H., and R. A. Bogomolni. 1994. Bacteriorhodopsin: a molecular photooscillator? *Chem. Phys. Lett.* 227:74–78.

Wu, S., and M. A. El-Sayed. 1994. Binding characteristics of an organometallic cation, Ru(bpy)3(2+), in regenerated bacteriorhodopsin. *J. Phys. Chem.* 98:7246–7251.

Zerner, M. C. 1990. Semiempirical molecular orbital methods. *In* Reviews in Computational Chemistry. VCH Publishers, New York. 313–365.

Zhang, Y. N., M. A. El-Sayed, M. L. Bonet, J. K. Lanyi, M. Chang, B. Ni, and R. Needleman. 1993. Effects of genetic replacements of charged and H-bonding residues in the retinal pocket on Ca^{2+} binding to deionized bacteriorhodopsin. *Proc. Natl. Acad. Sci. USA.* 90:1445–1449.

Zhang, Y. N., L. L. Sweetman, E. S. Awad, and M. A. El-Sayed. 1992. Nature of the individual Ca^{2+} binding sites in Ca^{2+}-regenerated bacteriorhodopsin. *Biophys. J.* 61:1201–1206.